SUPPORTING INFORMATION

The role of ion valence in the submillisecond collapse and folding of a small RNA domain

Suzette A. Pabit, Julie L. Sutton, Huimin Chen and Lois Pollack

Fluorescence anisotropy measurements show that Dy547 is not freely-rotating

In order to determine the collapse kinetics of tP5abc, we monitor the efficiency of Förster Resonance Energy Transfer (E_{FRET}) between a donor fluorophore (Fluorescein) and an acceptor fluorophore (Dy547, a dye that is spectrally similar to Cy3), attached to the tp5abc molecules of interest. E_{FRET} is related to the distance (R) between the donor and acceptor via:

$$E_{FRET} = \frac{1}{1+\left(\frac{R}{R_0}\right)^6} \quad \text{(S1)}$$

where R_0 is the distance at which E_{FRET}=1/2, known as the Förster radius. R_0 depends on κ^2, a factor representing the relative orientation of donor and acceptor transition dipoles. It is often assumed that the donor and acceptor are freely-rotating, giving rise to the case where κ^2=2/3, and one can obtain a value for R from a measurement of E_{FRET}. However, the presence of interactions between the fluorophores and the nucleic acid can make this assumption invalid, which precludes an accurate determination of R.

To determine the validity of the κ^2=2/3 assumption, we performed time-resolved fluorescence anisotropy measurements of the attached fluorescein and Dy547 using the time-correlated single photon counting (TCSPC) technique. The time dependence of the fluorescence anisotropy is a function of the rotational correlation time of the fluorophore which relates to its orientational freedom and hence κ^2. The anisotropy decay ($r(t)$) of a fluorophore linked to a macromolecule can be modeled by a two-component exponential (1):

$$r(t) = r_0\left(\alpha e^{-\frac{t}{\tau_F}} + (1-\alpha)\right)e^{-\frac{t}{\tau_M}} \quad \text{(S2)}$$

where r_0 is the fundamental anisotropy of the fluorophore, α is the is the fraction of depolarization due to fluorophore's internal motion, τ_F and τ_M are the rotational correlation times of the fluorophore and macromolecule respectively. For a freely rotating label α≈1 and $r(t)$ is dominated by the fast motion of the fluorophore while for a fixed label α=0 and $r(t)$ is dominated by the slow rotation of the macromolecule.

Measurements were performed on a custom fluorescence lifetime setup. Briefly, a 1060nm 80MHz laser (Fianium, Beverly, MA) was reduced to a repetition rate of 20MHz using a pulse picker (ConOptics, Danbury, CT). It was then frequency doubled to 530nm for Dy547 excitation. A 440nm 20MHz

Picosecond Diode Laser (Becker & Hickl, Berlin, Germany) was used to excite the fluorescein. A standard L-format arrangement (1) was used to measure fluorescence emitted perpendicular to the excitation path. Fluorescence emission polarized parallel and perpendicular to the excitation polarization was measured separately. Emission from the sample cuvette was collimated and filtered (495/20 and 635/50 band pass filters for fluorescein and Dy547, respectively), then focused onto a microchannel plate PMT (Hamamatsu, Bridgewater, NJ) for detection. A Becker & Hickl SPC-830 photon counting card was used for data acquisition. The anisotropy ($r(t)$) was calculated using:

$$r(t) = \frac{I_{VV}(t) - G\, I_{VH}(t)}{I_{VV}(t) + 2\, G\, I_{VH}(t)} \qquad \text{(S3)}$$

where $I_{VV}(t)$ and $I_{VH}(t)$ are the vertically and horizontally polarized emission, respectively, of the fluorophore with vertically polarized excitation. The G factor, a correction for the sensitivity of the detector at different polarizations, was calculated using the "tail matching" method (2) on free fluorescent dyes which have anisotropy decays much shorter than their lifetimes (Alexa fluor 488 for 440nm excitation and Rhodamine B for 530nm excitation).

The anisotropy decay of the A186U mutant in 25mM Mg^{2+} is shown in Figure S1. Similar trends were observed with no added salt and in 160mM K^+ (data not shown). From the fit to Equation (S2), the fluorescein decay is dominated by a fast component (α=0.68±0.03, τ_F=0.535±0.004ns, τ_M=6.9±0.3ns) indicating some rotational freedom. We also see rotational freedom of fluorescein in no added salt and in 160mM K^+ where we obtain α=0.73±0.02 and α=0.78±0.02, respectively. In contrast, the Dy547 decay is dominated by a slow component (α=0.287±0.007, τ_F=0.0614±0.0005ns, τ_M=19.0±0.2ns) indicating restriction of the fluorophore. Similarly, we measure constrained rotation of Dy547 with no added salt (α=0.178±0.006) and in 160mM K^+ (α=0.242±0.006).

This result is consistent with a scenario whereby Dy547 is rotationally constrained, likely due to stacking interactions with the nearby nucleotides in the P5c stem-loop. In fact, equilibrium fluorescence emission scans show the calculated E_{FRET} for both the tP5abc A186U mutant and wild-type decrease as a function of increasing ionic strength (Figure S5). Assuming a constant R_0, the decrease in calculated E_{FRET} would imply that the molecule becomes more extended as ionic strength is increased, contrary to the compaction observed by fluorescence correlation spectroscopy (FCS) and by comparison of the structures of the extended and folded states of tP5abc (3, 4). Due to the restricted motion of the Dy547, the actual value of κ^2 is unknown, hence E_{FRET} cannot be used to quantitatively measure distances between the donor and acceptor fluorophores. However, we do observe a change in E_{FRET} values between extended and compact conformational states. A set of control experiments (below) demonstrate that measured changes in fluorescence are the result of conformational changes and thus we can still use the time-dependent change in E_{FRET} to measure the collapse timescales of tP5abc.

Equilibrium fluorescence controls

To confirm that changes in E_{FRET} report the overall collapse of tP5abc, we examined the effect of salt concentration on the emission of free donor dye, free acceptor dye and directly excited labeled acceptor. Control experiments were performed by measuring the salt-dependence of fluorescence spectra using a Cary Eclipse Fluorescence Spectrophotometer. We measured the intensity dependence on salt concentration of free fluorescein and Dy547 under the range used for kinetic measurements (0, 30mM and 160mM K^+, and 0, 1mM and 25mM Mg^{2+}). The results show minimal intensity changes for free donor dye (Figure S6 A, B) and negligible changes in free acceptor dye (Figure S6 C, D).

From anisotropy data, we know that the donor fluorophore is freely rotating under all salt conditions ($\alpha \geq 0.68$), and thus we do not expect any significant changes in dye photophysics to influence the tP5abc donor intensity. Therefore, we focus our attention on how the RNA environment affects the acceptor dye. We measured the fluorescence resulting from the direct excitation of Dy547 attached to the A186U mutant (Figure S6 E, F). The decrease of Dy547 intensity when directly excited may indicate some quenching of the dye due to the change in dye environment after addition of salt. However, even after we correct the fluorescence intensity using the above results, we still observe a change in E_{FRET} upon the addition of salt. Taken together with FCS data indicating large scale collapse, these control experiments demonstrate that our measured changes in E_{FRET} are a consequence of overall collapse of tP5abc.

Microfluidic mixer experimental details

We used a microfluidic mixer design described in reference (5) to study the collapse of tP5abc RNA. This mixer was previously used to study fast protein folding kinetics (6). A schematic of the device is shown in Figure S2A. The RNA starts in a low-salt buffer and mixes with a higher ionic strength solution. The mixer uses hydrodynamic focusing (7, 8); faster flow velocities in the side channels containing the salt solution focus the slower RNA-containing center channel flow. The narrow sample jet at the mixing region facilitates fast diffusion of ions into the RNA sample. Flow in the two diagonal channels prevents pre-mixing of the side and center channels before the thin jet is formed. To demonstrate hydrodynamic focusing of the center channel flow, we show the fluorescence image of the 5-port mixing device in Figure S2B with Alexa 488-Dextran in the center channel, Alexa 405 dye in the diagonal channels and a non-fluorescent buffer solution in the side channels. The mixing region and upper part of the observation region is shown in the figure (boxed in white).

For our RNA collapse experiments, we use RNA concentrations of 4μM and flow rates of 10 μL/min in the side channels, 0.42 μL/min in the diagonal channels and 0.4 μL/min in the center channel. Flow is driven by syringe pumps (Harvard Apparatus, Holliston, MA). These flow rates were chosen to maximize mixer

stability. Prior to every measurement set, each device is characterized using KI quenching of Alexa 488-Dextran to determine the focused jet width and the mixing efficiency (5). The mixer performance is dependent on the focused jet width and the rate at which ions diffuse into the jet from the side channels (diffusion coefficients for the salt solutions used in this work are shown in Table S1). We define the mixing dead time as the time it takes for the ion concentration in the center channel to reach 1-(1/e) of its final value. For the above flow rates, the jet width was 1 μm, the mixing dead time for K^+ and Rb^+ ions was 140 μs, and that for Mg^{2+} and Sr^{2+} ions was 235 μs. Collapse of tP5abc is monitored by changes in the effective efficiency of energy transfer (E_{FRET}) between the two attached fluorescent labels (fluorescein and Dy547). As we have determined by fluorescence anisotropy measurements that Dy547 is not freely-rotating when attached to tP5abc (see above discussion), we are unable to use FRET as a "spectroscopic ruler" to measure of the actual size of the molecule. However, we are still able to use the changes in the effective E_{FRET} as an indication of molecular compaction. Fluorescent samples were imaged in the mixer using an Olympus Fluoview FV1000 BX61WI confocal microscope (Center Valley, PA) with an Olympus UAPO 20X water immersion objective. An excitation dichroic mirror (DM405/488/559) was used to separate laser scatter (at 488 nm) from the fluorescence signal while a SDM560 dichroic mirror was used to separate the donor and acceptor signals. Two additional emission filters BA505-525 and BA575-675, were used for the donor and acceptor channels, respectively. We simultaneously collected donor channel (D_{ch}) and acceptor channel (A_{ch}) images using the Olympus Fluoview software and used Matlab (Natick, MA) for image analysis and fitting. We calculated $E_{FRET} = A_{ch}/(D_{ch} + A_{ch})$ from fluorescence intensities measured per laser scan. E_{FRET} from a set of at least 100 fluorescence images of the mixer were averaged for each buffer condition. Numerical simulations of flow speed in the mixer using COMSOL Multiphysics (Burlington, MA) were used to convert the distance along the outlet channel to the time after mixing (5).

REFERENCES

1. Lakowicz, J. R. 2006. Principles of fluorescence spectroscopy. 954.

2. O'Connor, D. V.and D. Phillips 1984. Time-correlated single photon counting. Academic Press, London.

3. Zheng, M., M. Wu and I. Tinoco Jr 2001. Formation of a GNRA tetraloop in P5abc can disrupt an interdomain interaction in the tetrahymena group I ribozyme. Proc. Natl. Acad. Sci. U. S. A. 98, 3695-3700.

4. Cate, J. H., R.L. Hanna and J.A. Doudna 1997. A magnesium ion core at the heart of a ribozyme domain. Nat. Struct. Biol. 4, 553-558.

5. Park, H. Y., X. Qiu, E. Rhoades, J. Korlach, L.W. Kwok, W.R. Zipfel, W.W. Webb and L. Pollack 2006. Achieving uniform mixing in a microfluidic device: Hydrodynamic focusing prior to mixing. Analytical Chemistry. 78, 4465-4473.

6. Park, H. Y., S.A. Kim, J. Korlach, E. Rhoades, L.W. Kwok, W.R. Zipfel, M.N. Waxham, W.W. Webb and L. Pollack 2008. Conformational changes of calmodulin upon Ca2+ binding studied with a microfluidic mixer. Proc. Natl. Acad. Sci. U. S. A. 105, 542-547.

7. Knight, J. B., A. Vishwanath, J.P. Brody and R.H. Austin 1998. Hydrodynamic focusing on a silicon chip: Mixing nanoliters in microseconds. Physical Review Letters. 80, 3863-3866.

8. Pollack, L., M.W. Tate, N.C. Darnton, J.B. Knight, S.M. Gruner, W.A. Eaton and R.H. Austin 1999. Compactness of the denatured state of a fast-folding protein measured by submillisecond small-angle x-ray scattering. Proc. Natl. Acad. Sci. U. S. A. 96, 10115-10117.

9. Haynes, W. M.and D. R. Lide 2011. CRC handbook of chemistry and physics: a ready-reference book of chemical and physical data. CRC Press, Boca Raton, FL.

Salt	Diffusion Coefficient ($\times 10^{-5}$ cm^2 s^{-1})
KCl	1.994
RbCl	2.052
$MgCl_2$	1.250
$SrCl_2$	1.334

Table S1: Diffusion coefficients of salt solutions used in microfluidic mixing experiments (9)

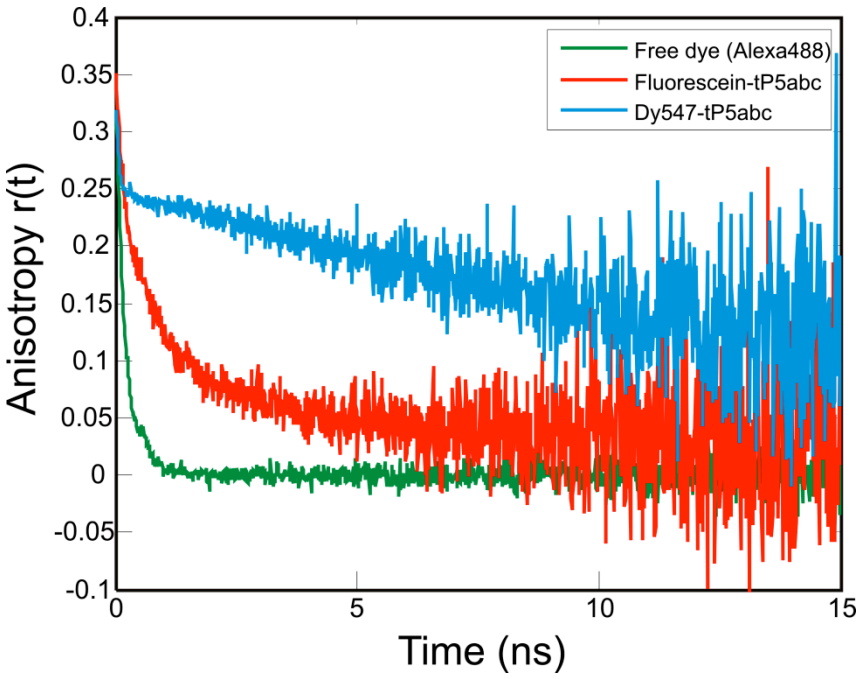

Figure S1. Time-resolved fluorescence anisotropy decay of the fluorophore-labeled tP5abc A186U mutant in 25mM Mg^{2+}.

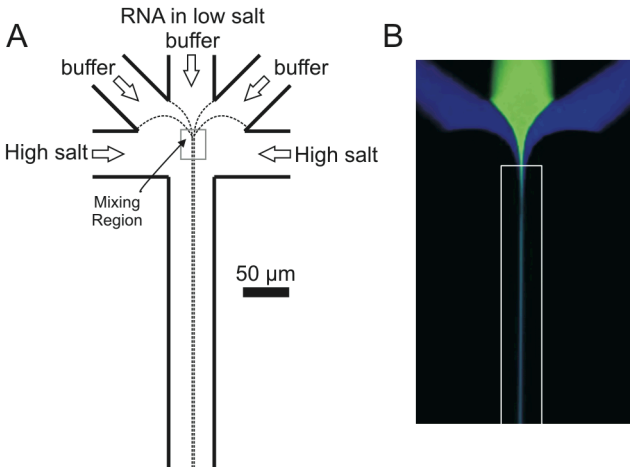

Figure S2. We used a microfluidic mixer to change the ionic conditions and trigger RNA collapse. (A) A schematic of the mixing device. RNA in a low salt buffer (in the center channel) is rapidly mixed with a solution that contains the same buffer with added salt (in the side channels). Hydrodynamic focusing due to the fast-flowing side channels causes the narrowing of the center channel flow, facilitating fast diffusion of ions. Mixing uniformity is further improved by preventing premixing using flow of low salt buffer in the diagonal channels. Dashed lines represent a typical outline of flow patterns. All channels have a width of 50 µm and a depth of 100 µm. (B) A composite fluorescence image of flow in the mixer with Alexa 488-Dextran in the center channel, Alexa 405 in the diagonal channels and buffer (non-fluorescent) in the side channels. The white box shows the beginning of the observation region where kinetic traces are acquired.

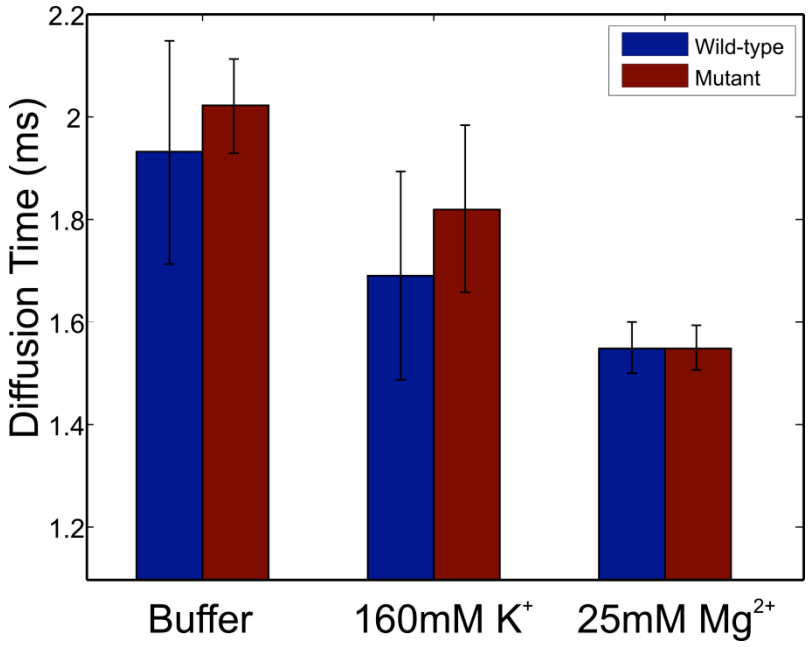

Figure S3. Diffusion times (τ_D) of both the A186U mutant (blue) and the wild type tP5abc (red) as measured by FCS. Wild-type tP5abc and A186U mutant diffusion times are indistinguishable. Similar to the discussion in the text, we see a decrease in τ_D with the addition of salt (160mM K^+ or 25mM Mg^{2+}) in the wild type, which demonstrates the electrostatic relaxation of the molecule. Within the limitations of FCS, we cannot resolve differences between the folded state of the wild type when Mg^{2+} is present and the collapsed state of the mutant. The data in Figure S3 were taken with a different focal volume as the data shown in Figure S4, and in Figure 2B and C of the main text, and so differ slightly.

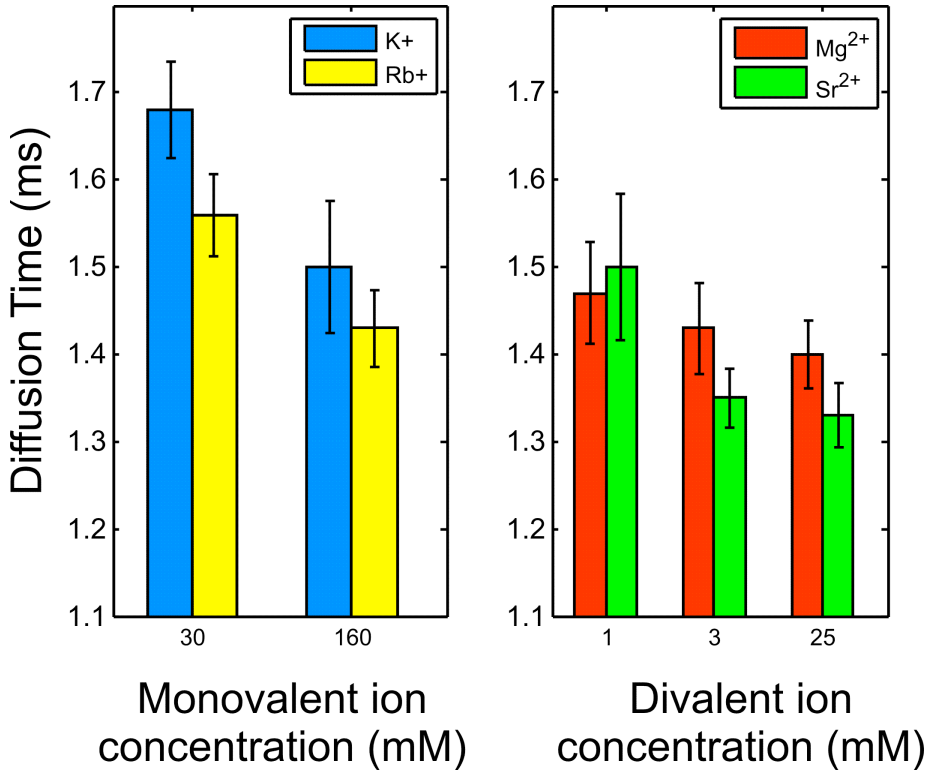

Figure S4. Dependence of A186U mutant diffusion time on ion type. We used FCS to measure τ_D for the A186U mutant under conditions with different ion types. As before, we see a decrease in τ_D for increasing salt concentration. Similar to the results of second virial coefficients (Figure 1A), we cannot distinguish between K^+ and Rb^+ or between Mg^{2+} and Sr^{2+}. This result is consistent with the picture that the ion type does not affect the electrostatic collapse of tp5abc for a given ion valence.

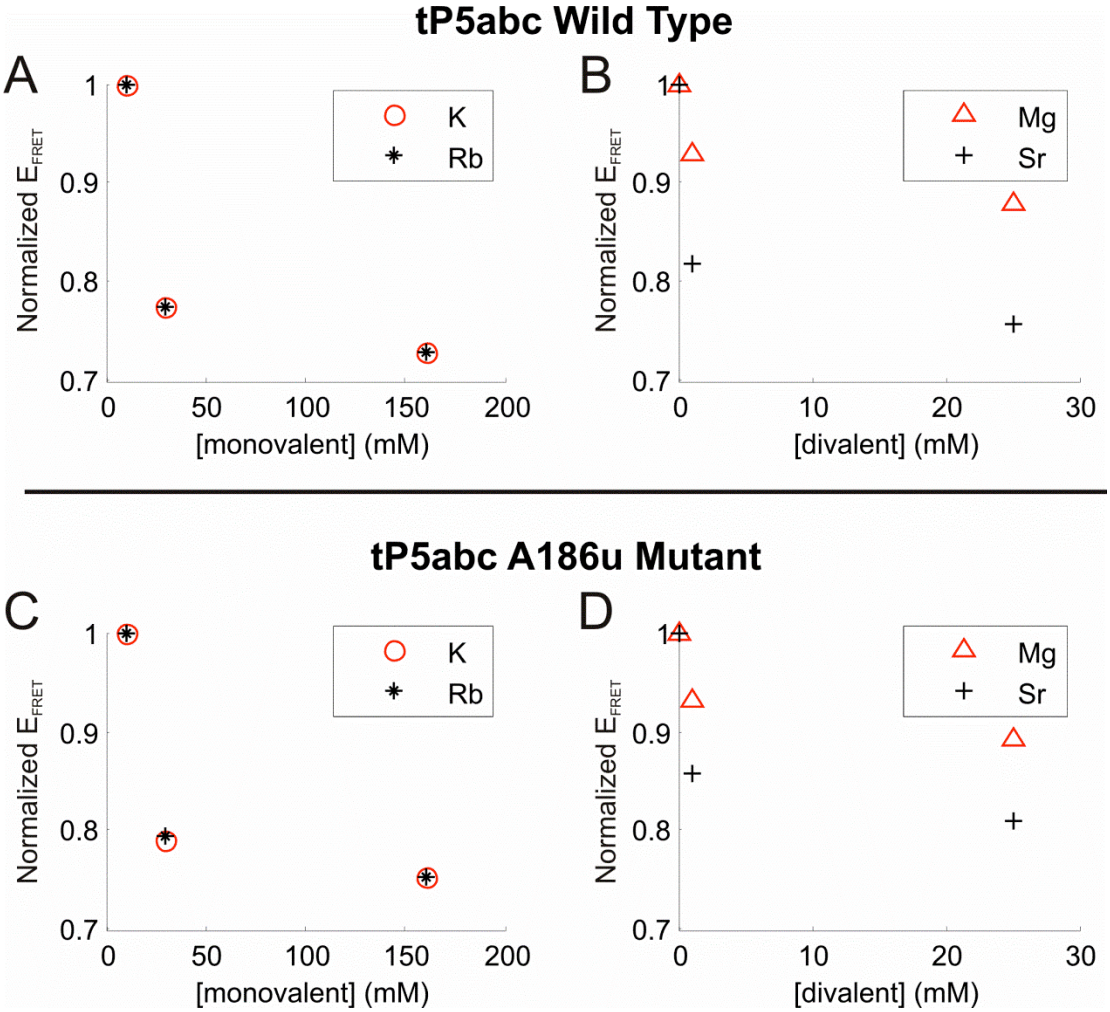

Figure S5. Equilibrium FRET measurements for the tP5abc wild type (A,B) and A186U mutant (C,D). E_{FRET} was calculated as $A/(A+D)$ were A and D are the peak vales of acceptor and donor fluorescence emission, respectively. It was then normalized by the E_{FRET} measured with no added salt analogous to data taken in the mixer. Since the acceptor dye is not freely rotating, E_{FRET} cannot be interpreted as an intramolecular distance.

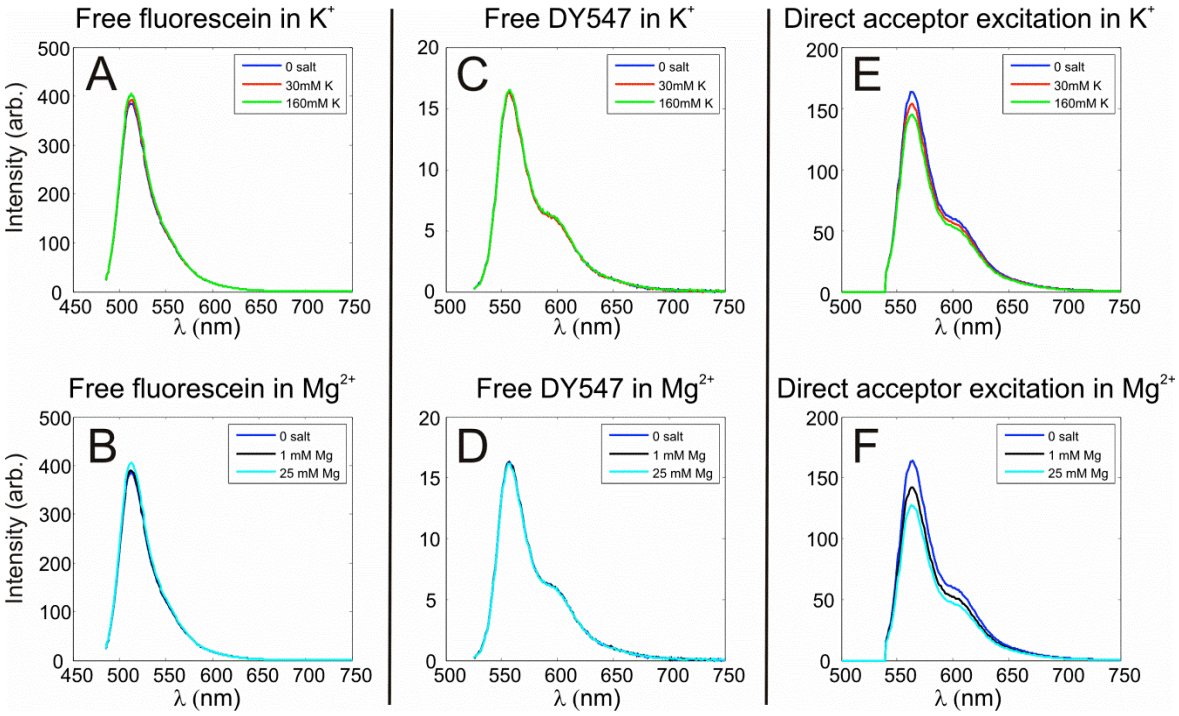

Figure S6. Change in fluorescence intensity as a function of salt concentration for free donor dye (A, B), free acceptor dye (C, D) and directly excited acceptor dye in the A186U RNA mutant (E, F). The top panels represent monovalent ions while the lower panels use divalent ions.